Topological data analysis for roughness surfaces of bonding assembly

Helene Canot, Philippe Durand, Emmanuel Frénod, Bouchra Hassoune-Rhabbour, Valérie Nassiet, Olivier Tramis

Topological data analysis for roughness surfaces of bonding assembly

Hélène Canot*[1], Philippe Durand[2], Emmanuel Frénod[1], Bouchra Hassoune[3], Valérie Nassiet[3] and Olivier Tramis[3]

[1]Université de Bretagne-Sud, UMR 6205
Laboratoire de Mathématiques de Bretagne Atlantique, F-56000 Vannes, France

[2]CNAM, Département de Mathématiques et Statistiques
M2N, 292 rue Saint Matin, 75141 Paris cedex, France

[3]Laboratoire Génie de Production at UTTOP
47 Av. d'Azereix 65000 Tarbes, France

Abstract

Testing the reliability of bonded joints in material assemblies is one of the major subjects in the aeronautical industry. One of the methods for characterizing adhesion is based on the study of the roughness of the fracture surfaces of assemblies. In this study, the interest is focused on the quantification of the adhesion of the bonded structure by the corner cleavage test, allowing the study of crack propagation within bonded assemblies. Optical profilometry measurements, obtained by scanning the surface of the fractured surfaces of monoadhesives: ABT M52, copolymer-doped and non-nanostructured AHT are used. The aim of the profilometric study is to quantify surface roughness. To go further than traditional methods of characterizing roughness, we analyze the profiles using mathematical methods to confirm the experimental studies and extract more geometric information. We apply various techniques of topological data analysis (TDA) to extract the topological features of the profiles. These techniques recover experimental elements in a quantitative manner. Persistence diagrams give us a multi-scale characterization of the rupture facies, attesting the voids, micro-cracks at nano-level, quantifying the maximum amplitude of the peaks at micro level. We extract features vectors using persistent images for each profile and we look for similarities in persistence diagrams using Bottleneck and Wasserstein distances in perspective of a machine learning application in a future study. Then the profiles were studied by Takens embedding which will produce a point cloud analyzed by homological persistence in order to produce indications of periodicity or quasi-periodicity. This computational topological approach makes it possible to extract the essential characteristics of the

surface and roughness of the profile of the adhesives in order to conclude on their toughness and fracture resistance.

Keywords -Roughness, topological data analysis, persistence diagram, homology, tenacity, adhesion, bonded assembly.

1 Introduction

Structural bonding to assemble different materials has become a major technique in the industrial world because it is interesting in terms of the cost of lightening structures and aesthetics. However, the increase in the interval of use of the seal in temperature remains a source of very pragmatic scientific problem. New joint concepts whose properties are continuous along the bonded surface have emerged. An adhesive joint, whatever its nature, must be reliable in time and in service. The adhesion of the mono-adhesive joints and of the joint with a gradient of properties by a corner cleavage test is studied. The role of an adhesive joint is to ensure a continuous transfer of stresses between the different materials that it assembles Hartshor [18]; Bolger et al. [5]. However, it is the glass transition temperature (Tv) of the adhesive that determines the temperature range for which the bonded assembly can be used. For a temperature well below its Tg, the adhesive is in a glassy and brittle state. For a temperature well above its Tg, the adhesive is in a rubbery and flexible state. In both cases, the adhesive cannot provide optimal stress transfer.

The durability of the assembly can therefore only be ensured within an interval around its Tv. This interval is called the Zone of Optimal Resistance. When the service temperature falls within the ZRO of the adhesive, the latter has an optimal ductility-stiffness couple. A bonded assembly will only perform well over this limited temperature range. However, Hart-Smith [20] proposed the concept of the Multi Adhesive Joint (JMA) in order to be able to extend the ZRO of a bonded assembly. It is enough to combine in the same joint two or more adhesives having different ZRO. A high temperature adhesive (AHT) is combined with a low temperature adhesive (ABT). The combination of the ZROs of ABT and AHT gives the Multi Adhesive Joint an optimum resistance zone that extends from low to high temperatures. Indeed, if the temperature is close to the Tg of the ABT adhesive, the two adhesives participate in the transfer of charges between the substrates, the AHT thanks to its high modulus and the ABT thanks to its ZRO. If the temperature is close to the Tg of the AHT adhesive, only the AHT ensures the transfer of charges between the substrates. The ABT is far from its ZRO and its modulus is too low to participate in the resistance of the whole. Thus, this combination should ensure better behavior of the bonded assembly over a wider temperature range.

Structural adhesives are often brittle below their glass transition temperatures. One way to make them more tenacious is to make them more flexible, by micro-structuring them. Adding particles (based on rubber, clay or thermoplastic polymers) allows the adhesive to dissipate more energy during crack propagation and increases the toughness of the adhesive. By microscopic observation of fracture patterns of mixtures of epoxy adhesives and silicone particles, Pearson et al (Yee et al. [33]; Pearson et al., 1991 [23]; Pearson et al., 1993 [24]) list 4 crack propagation regimes: The crack can be trapped by the particles (crack pinning). Trapping is due to a difference in toughness between the matrix and the particles. The presence of particles can deflect the crack, if not trap it. The surface created is greater when the crack is deflected, which explains the increase in toughness. The crack can in this case separate into several branches, which further increases the surface created by its passage. Microcracks, located around the particles upstream of the crack head. Particles can also plasticize upon loading. On the one hand, this plasticization phenomenon can cause a drop in their Young's moduli, which creates a contrast with the matrix and causes a stress concentration at the particle level. This phenomenon leads to the appearance of shear bands in the matrix, mechanisms allowing a significant dissipation of energy during loading, which results in an increase in toughness. The particles can cavitate, creating cavities (voids) in the matrix which increase the surface created by the passage of the crack.

One of the solutions to obtain a structuring at the submicron scale lies in the addition of thermoplastic copolymer. Indeed, the nano-structuring is done in this case by self-organization of the copolymers in the epoxy matrix. The addition of copolymers to an AHT adhesive, chosen for its high Tv, makes it possible to obtain an ABT adhesive, with higher tenacity but an equivalent Tv. A wedge cleavage test on the adhesives is initiated in order to assess their durability by studying their resistance to fracture. The roughness of the various surfaces is studied on the raw profiles of cracked facies. Figures 2 show crack facies and corresponding profiles from O. Tramis' experiments [31]:

The main idea of this paper is to analyze these raw profiles by topological data analysis methods, in particular with the use of persistent homology, images persistence, Bottleneck and Wasserstein distances, sliding window embbeding method.

Many physicists have been interested in the adhesion of assemblies with in particular the corner cleavage test. Cognard [11] uses the wedge cleavage test in an aggressive medium to show that it is the driving force behind crack propagation. This test is commonly used to study the durability of bonded assemblies see Hart-Smith, [21]. An assembly is then considered to be durable if the crack remains cohesive in the adhesive throughout aging, and does not propagate. In addition to the quality control test, this test

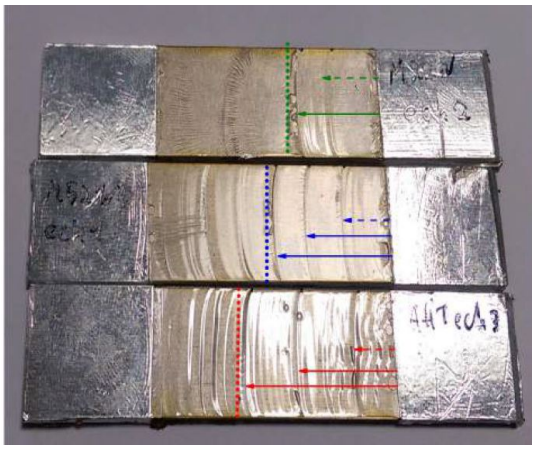

Figure 1: Cracked facies for the AHT and ABT M52 assemblies. The crack stopped at the dotted line, for each assembly.

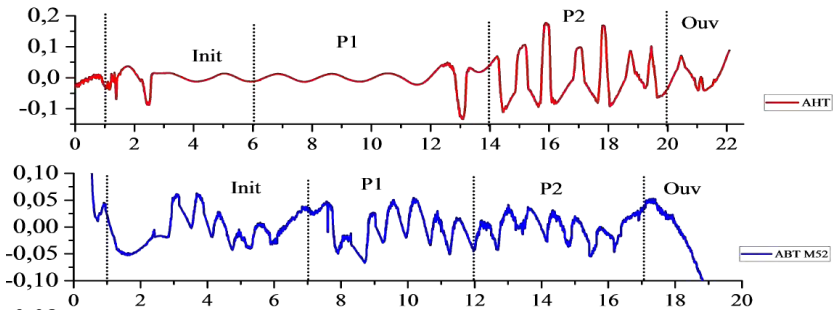

Figure 2: Profiles measured by optical profilometry of AHT and ABT M52 assemblies.

also allows to study the evolution of an interface according to the type of environment. It is one of the rare mechanical tests to be able to discriminate between two different surface treatments, with identical adhesives and substrate. In the same way, this test is adapted to the discrimination of adhesives, with identical substrates and surface treatment see Armstrong, [2]. The wedge can be inserted continuously into the assembly [13]. The substrates constantly experience loading, which causes several advances of the crack. Moreover, the crack jumps are constant if the crack remains in the adhesive throughout the test. Indeed, when the crack is at a standstill, the wedge must be pushed in a certain amount to cause a crack jump. Once this depth is reached, the crack propagates. To propagate the crack again, the wedge must be pushed in an equivalent amount, which will cause a new crack jump. With regard to the fracture surfaces of the assemblies, Chen et al [10] were interested in the surface condition of the adhesives during crack jumps. They showed that, during tests favoring a tensile opening mode, an unfilled adhesive presented a corrugated fracture surface; For filler concentrations close to 10%, the fracture surface of a filled adhesive is less wavy. This change in surface topography is attributable to the stability of crack propagation. This stability depends on the phase angle $\tan^{-1}(K_{II}/K_I)$, which reflects the aperture mode mix. The smaller this angle, the more the crack propagates in a straight line (smooth facies). The bifurcation of the crack (wavy facies) therefore results from a mix of modes at the crack head.

Roughness is an essential characteristic of the state of a surface. Concretely, the study of the profile of the fracture facies is an effective means of quantifying the surface roughness and its influence on the adhesion of the assemblies. Roughness profiles with many non-stationary characteristics of high-performance mathematical methods are necessary in order to precisely characterize the topography of surfaces according to the properties of assemblies. Known and well-honed measurement techniques in order to characterize a profile, make it possible to measure the peaks and troughs recorded over a given length and calculate the roughness parameters such as: Ra, Rt, Rz. Where the arithmetic mean roughness Ra is the absolute average of the profile values. The maximum profile height Rz indicates the absolute vertical difference between the maximum height of the peaks and the maximum depth of the valleys of the profile and total profile height. Rt indicates the vertical difference between the maximum peak height and the maximum valley depth over the profile.

The experimental study was carried out during Olivier Tramis' thesis [31], all the data in this article come from his thesis work. The maximum amplitudes of the roughness peaks of the profiles were calculated during his work. We then wanted to apply a mathematical method based on the topological analysis of [8] data on these roughness profiles in order to reinforce the experimental results and learn additional information. Persistent ho-

mology enables rapid and robust analysis of complex data such as fracture profiles. Its advantage is that it allows to characterize objects on large and small scales.

In particular, persistence diagrams which summarized the outputs persistent homology, are introduced in order to quantify micro and nano-level peaks, voids and micro-cracks, all the topological structures of the fracture facies. They group together a set of points, each point of which defines the voids, cavities, peaks which are born at the abscissa x and disappear at the ordinate y. Homological persistence has already been shown to be a robust descriptor of roughness characteristics. Yesilli et al. [34] proposed an automatic feature extraction from profiles surface with TDA based approach to determine the level of roughness. Comparing its performance to traditional method, their TDA based approach outperform the traditional signal processing tools. Senge et al. [27] described the evolution of surface topography for different shot peened surface usibg TDA. They demonstrate the avantage of using persistence based parameters relative to existing surfaces roughness parameters. In additional Machine Learning method Hasan et al. [19] applied TDA for analysing surface roughness at macro and nano scales. TDA is used for analysing the contact of roughness surfaces. In [14] Duman et al chose topological data analysis to describe hydrophobic surfaces and extract morphological features from the AFM images.The voids, spherulites and fibrils of the crystallized polycarbonate (PC) surface studied are summarized and quantified in the persistence diagrams. They extract feature vectors for each persistence diagram using Bendich's method for further use in PCA and K means algorithms. These clustering methods shown that the surfaces with high contact angle lie in the same cluster. In [32] Yamamoto analyzes surface roughness using persistence diagrams by focusing on the life spans of the islands and lakes, which follow power law distribution where the scaling exponent vary according to the roughness of the surface.

This paper is organized as follows: In section 2 we will give an introduction to persistent homology as well as the different TDA techniques used. Section 3 will focus on describing the experimental scope as well as the methodology used. Section 4 is devoted to the results of the topological study of adhesive profiles using persistence diagrams as well as the geometric structure of sliding windows embedding from the profiles. Finally in section 5 we will conclude and open up to some perspectives.

2 Mathematical background

We describe the persistent homology analysis that we use in our study. We present the general mathematical definitions necessary for the study of profiles.

2.0.1 Simplicial homology

Let V be a set of vertices, a *simplicial complex* on V is a set K composed of subsets of V (the simplices) such that any $\tau \in \sigma$, nonempty, $\tau \in K$. the dimension of a simplex $dim(\sigma)$ is the number of vertices of σ minus 1.

$K = \{0, 1, 2, 3, [0, 1], [1, 2], [0, 3], [0, 1, 3]\}$ is a simplicial complex.

If K is a *simplicial complex*, we denote by K_n the set of simplices of dimension n, we define the n-chains of K, these are linear combinations of n-dimensional simplexes, It is convenient to work on the field $(\mathbb{Z}/2\mathbb{Z}, +, x)$ of integers modulo 2. Thus the n-chains are written formally by:

$$c = \sum_{\sigma \in K_n} \epsilon_\sigma . \sigma, \text{ with: } \epsilon_\sigma \in \mathbb{Z}/2\mathbb{Z} \tag{1}$$

and form vector spaces over the field $\mathbb{Z}/2\mathbb{Z}$.

We can define the boundary of the n-dimensional simplex $\sigma_n = (p_0, p_1, ...p_n)$:

$$\partial_n \sigma_n = \sum_{i=1}^{n} (p_0, p_1, ..., \widehat{p_i}, ...p_n) \tag{2}$$

The operator ∂_n expands to a linear map from $\mathcal{C}_n(K)$ to $\mathcal{C}_{n-1}(K)$ We can verify that the boundary of the boundary of a simplex is zero:

$$\partial_{n-1} \circ \partial_n = 0 \tag{3}$$

For exemple:

$$\partial \circ \partial([1, 2, 3]) = \partial([1, 2] + [2, 3] + [1, 3) = 1 + 2 + 2 + 3 + 1 + 3 = 0$$

A vector space sequence:

$$... \longrightarrow \mathcal{C}_n(K) \xrightarrow{\partial_n} \mathcal{C}_{n-1}(K) \xrightarrow{\partial_{n-1}} \mathcal{C}_{n-2}(K)... \xrightarrow{\partial_0} \mathcal{C}_0(K) \longrightarrow O \tag{4}$$

is a complex simplicial. The kernel and image of each linear map, ∂_n are vector subspaces, the n-cycles: $Z_n(K)$ represent the kernel of δ_n: $Ker(\partial_n)$, the n-edges: $B_n(K)$ the image of δ_{n+1}: $Im(\partial_{n+1}$. We have the inclusion: $B_n(K) \subset Z_n(K)$. A topological defect is the obstruction for an n-cycle to be an n-boundary: it results in the non-nullity of the quotient vector space (homology vector space $H_n(K)$) given by:

$$H_n(K) = Z_n(K)/B_n(K) = Ker(\partial_n)/Im(\partial_{n+1}) \tag{5}$$

The dimension of each $H_i(K)$ is denoted: $\beta_i(K) = dim(H_i(K))$ and represent the betti numbers of the complex K.

The n-th vector spaces of homologies are finer invariants than the fundamental group. Indeed the fundamental group of a point and a sphere are

identically null: any loop, drawn on a sphere, can be retracted on a point. Yet there is no homotopy retracting a sphere on a point, nor even a homeomorphism. On the other hand, the second homology vector space of the point is zero while that of the sphere is non-zero: the sphere is not a boundary because it has no interior. The homology vector spaces of a *simplicial complex* are easily computable: we do linear algebra and matrix calculus, this explains why it is these invariants that are used in practice.

2.1 Topological data analysis

Data analysis is to the study of a cloud of points in a Euclidean space. The topological analysis of the data leads, to associate with the point cloud of a *filtration* of *simplicial complexes* in order to calculate the invariants which are the spaces of homologies of all dimensions, as well as the Betti numbers which represent the dimensions of these spaces. Let us recall that the fact of showing homology amounts to detecting all the independent cycles which are not edges. *Filtration* is obtained by thickening the cloud of points by considering the balls of epsilon rays around each of them. At the beginning, the balls are very small and do not intersect. The topology is simple, the *simplicial complex* contains only points and the topology comes down to count the number of points corresponding to connected components. Then, when epsilon increases, the balls around each dot begin to intersect.

If two balls intersect, we add an edge between their center, we build what we call the nerves of the covering see Figure 3. If the intersection of three balls is not empty, we add the simplex constituted by each of the centers of these three balls etc...

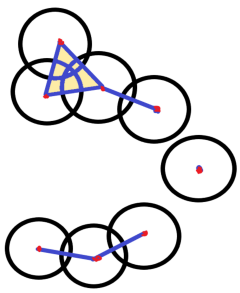

Figure 3: Nerve of cover

For each value of increasing epsilon, we can therefore associate a simplicial complex and calculate the homology at the resolution epsilon. We will keep in this evolution, persistent homology see Fig 4. It will report the topology of the point cloud. This is used in the rest of this article, to

interpret the analyzed data.

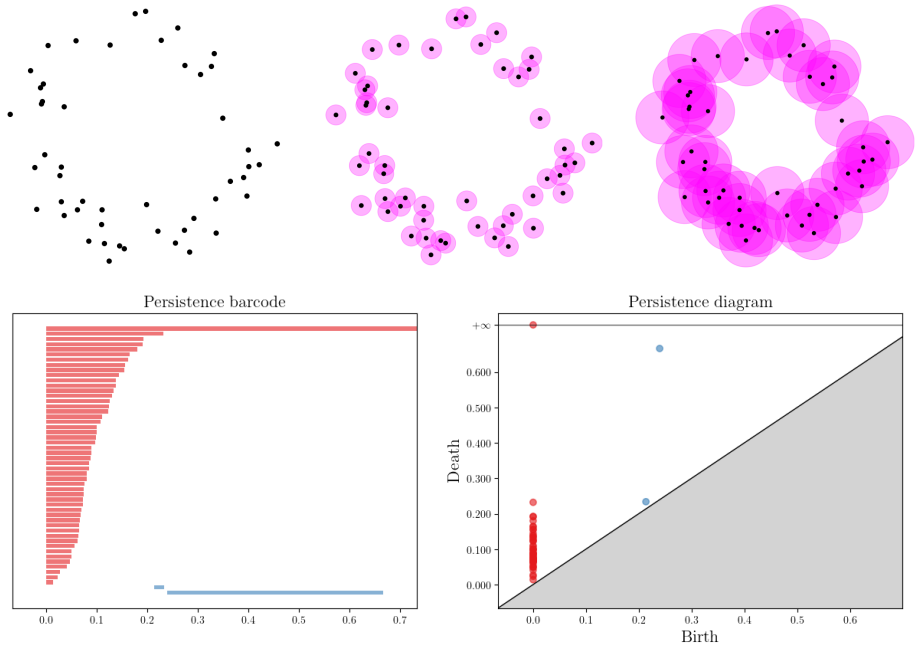

Figure 4: Filtration showm with increasing values of ϵ (top), bottom is the corresponding persistent barcode on the left and persistence diagram on the right. Each red bar and each red point in 0-dimensional represent the connected components, the blue barcode and the blue points in 1-dimensional represent the holes

Definition 2.1 *(Nerve cover) Let be X a topological space, a cover of X is given by the data $\mathcal{U} = (U_i)_{1 \leq i \leq N}$ such that* $\bigcup_{1 \leq i \leq N} U_i = X$.

The nerve of $\mathcal{U}$ is the simplicial complex with vertex $\{1, ...N\}$ and m-simplices are the subset $\{i_1, ...i_m\} \subset \{1, ...N\}$ with $\bigcap_{k=0}^{m} U_{ik} \neq \emptyset$.

Now we introduce the principle of the Vietoris Rips complex that we will use in our homological persistence calculations. The *Vietoris-Rips Complex*, contains simplices of bounded dimension.

Definition 2.2 *(Vietoris-Rips Complex) Given $\epsilon > 0$, the Vietoris-Rips complex $VR(X, \epsilon)$ with vertex set X and the parameter ϵ is defined by:*

$$\{x_1, x_2, ...x_k\} \in VR(X, \epsilon) \quad \Leftrightarrow \|x_i - x_j\| \leq \epsilon$$

for all $i, j \in \{0, 1, ..., k\}$.

A filtration of a simplicial complex K*, is a nested sequence of subcomplexes starting at the empty set and ending with the full simplicial complex, i.e.,*

$$\varnothing \subset K_0 \subset K_1 \subset ... \subset K_n = K \tag{6}$$

Then going back to the Rips complex

Definition 2.3 *(Vietoris-Rips filtration) As* ϵ *goes to 0 from* ∞ *the nested sequence of Rips complexes* $VR(X, \epsilon)$ *defines the Vietoris-Rips filtration.*

2.1.1 Persistence module

We consider an increasing thickening sequence of X that denote a filtration:

$$X^{0,0} = X \subset X^{0,1} \subset X^{0,2} .... \subset X^{0,k} .... \tag{7}$$

We have the functor: $X^{0,l} \to H_i(X^{0,l})$ acting from the category of sets in the category of i^th-homology vector spaces. We calculate for each thickening $X^{0,l}$ Betti numbers,

$$\beta_0 = dim(H_0(X^{0,l})), \beta_1 = dim(H_1(X^{0,l})), \beta_i = dim(H_i(X^{0,l}))...$$

At the sequence of inclusions:

$$X^{0,0} \overset{i_0^1}{\hookrightarrow} X^{0,1} \overset{i_1^2}{\hookrightarrow} X^{0,2} \overset{i_2^3}{\hookrightarrow} X^{0,3} \overset{i_3^4}{\hookrightarrow} X^{0,4} ... \tag{8}$$

it corresponds by applying rhe i^th homology functors:

$$H_i(X^{0,0}) \overset{(i_0^1)_*}{\longrightarrow} H_i(X^{0,1}) \overset{(i_1^2)_*}{\longrightarrow} H_i(X^{0,2}) \overset{(i_2^3)_*}{\longrightarrow} H_i(X^{0,3}) \overset{(i_3^4)_*}{\longrightarrow} H_i(X^{0,4}) ... \tag{9}$$

To the inclusion, corresponds linear map between vector spaces, in the second sequence, we obtain a persistence module given by the sequence of vector space:

$$(H_i(X^{0,l}))_{l \geq 0},$$

with linear maps

$$((i_k^l)_* : H_i(X^{0,k}) \to H_i(X^{0,l}))_{l \leq k}$$

We can define the persistence: Let $i, k_0 \geq 0$, and consider a cycle $c \in H_i(X^{0,k_0})$.

Its death time is: $sup\{k \geq k_0 / (i_{k_0}^k)_*(c) \neq 0\}$.

Its birth time is: $inf\{k \geq k_0 / (i_k^{k_0})_*^{-1}(c) \neq 0\}$.

Its persistence is the difference:

$$P(c) = sup\{k \geq k_0 / (i_{k_0}^k)_*(c) \neq 0\} - inf\{k \geq k_0 / (i_k^{k_0})_*^{-1}(c) \neq 0\} \tag{10}$$

2.1.2 Morse homology

In our context, persistent homology (persistent diagrams, lifespan, persistent images ...) has been adapted to function graphs representing profiles. Thanks to Morse theory [15] which studies the topology of sublevel sets for generic functions on simplicial complexes. It is interested in the critical points of a numerical function. We consider a function of a real variable, we are interested in the critical points that are not concretely degenerate, the extrema of a function. Especially, we are interested in sets of sublevels of f i.e. $\mathbb{R}_t = f^{-1}(]-\infty, t])$. For a numerical function of a real variable, the topology of the sets of sub-levels is captured by the connectivity when we meet a minimum, an interval splits into two connected components. On the other hand, when we pass by a maximum, two connected components merge. We thus still have a notion of persistence: the time which separates the creation of a new connected component named the *birth time* and its disappearance named *death time*, and the persistence or lifespan is the difference between its death and birth time. Persistence diagram consists of a one-to-one minimum-maxixum pairing see fig 5. In this paper, it is this functional approach which is privileged. To illustrate this approach we consider the sublevels of the function of a single real variable: $f : I \to \mathbb{R}$ illustrated by the graph below:

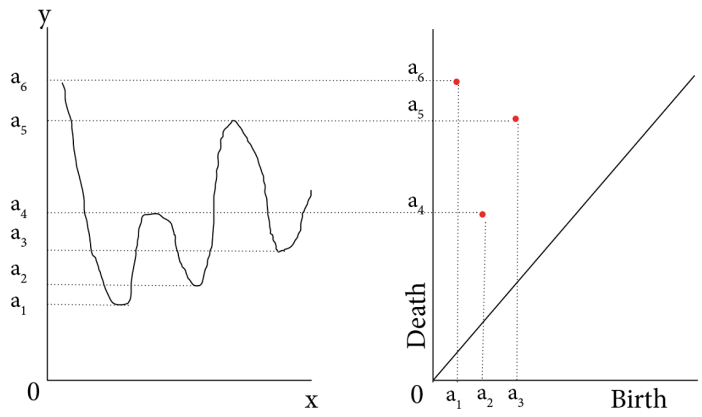

Figure 5: On the left example of a profile and on the right 0-th persistence diagram associated.

We study the spaces : $f^{-1}(]-\infty, a])$ according to the growth of the real a. On passage of a_1 a first connected component is created, then a second on passage of a_2 and a third on passage of a_3. The second connected component a_2 disappears in a_4, the two components a1 and a_2 merge, only one remains. Then the component a_3 disappears in a_5, the two values are

paired and called "*the persistent pair*" and are represented by a point in the persistence diagram of the Figure 5. The persistence interval is therefore the lifetime of the component a_3 up to a_5. Finally, the persistence diagram is given by interval: $D = \{(a_1, a_6), (a_2, a_4), (a_3, a_5)\}$.

2.1.3 Lifetime diagram and persistence image

Directly reading a persistence diagram for roughness profiles is not straightforward due to the complexity of the structure. So we extract feature from persistence diagrams using different methods. We construct lifetime diagram $\mathcal{T}$ and its vector representation called persistent image. Fig 6 illustrate our method of computational persistence diagram and lifetime diagram for AHT P1 profile. The persistent diagram in 0-dimensional and 1-dimensional describes the coordinate pairs (a_i, b_i) which represent the birth and death height of each peaks. We evaluate the maximum amplitude of a peak thanks to the lifetime diagram. Each point of the persistence diagram (a_i, b_i) (on the left) is projected onto Euclidean plane (right) via the linear transformation $(a_i, b_i - a_i)$, where $b_i - a_i$ is the lifetime of a peak.

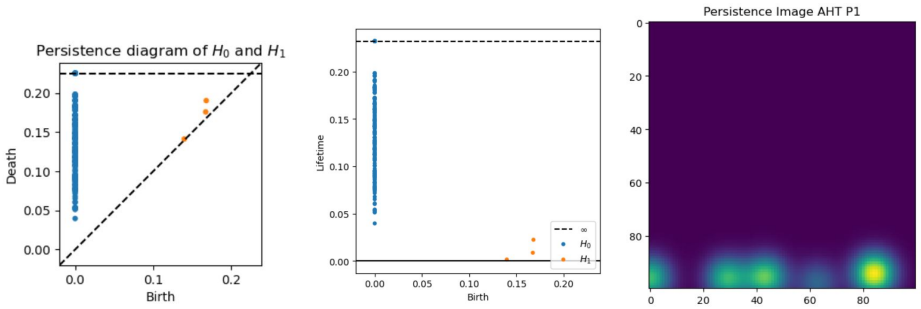

Figure 6: Persistent diagram (left) converts to lifetime diagram (middle) and its persistence image (right)

Next, we construct a persistent image by considering a continuous piecewise derivable non-negative weighting function :

$$\omega(a_k, p_k) = \begin{cases} 0 & p_k \leq 0 \\ p_k/p_{max} & 0 \leq p_k \leq p_{max} \\ 1 & p_{max} \leq p_k \end{cases} \tag{11}$$

where p_k is the lifetime of the points in the diagram [1] and a normal distribution centered at each point of the transformed diagram, with its variance σ, $\sigma > 0$. Then the persistence image is expressed, using the weighting

function and the normal distribution, by

$$S(x,y) = \sum_{(a_k,p_k)\in\mathcal{T}} \omega(a_k,p_k) g_k(x,y) \tag{12}$$

We fix a grid in the plane with n pixels and award to each the integral of S over that region. The persistent image see Fig 6 is the integral of the persistent surface over the grid and pixel values :

$$I_{i,j}(S) = \int\int S(x,y)dxdy. \tag{13}$$

3 Methods

3.1 Experimental perimeter

The assemblies are made, for these cleavage tests, with 2017 aluminum substrates. A chamfer at the start of the assembly allows facilitate the insertion of the wedge during the test. Before gluing and assembly, the substrates are degreased to remove grease and dust present on the surface of the substrates, as well as to eliminate traces of surface oxides. An assembly prepared with simply degreased substrates will be denoted SD assembly. Some substrates undergo a surface treatment after cleaning: phosphoric anodization denoted SA. The substrates are then glued: only one of the substrates is glued. To perform continuous wedge cleavage tests on AHT, ABT M52 assemblies, a crack is initiated by inserting the 0.7 mm thick wedge. Once the crack has started, the wedge is removed and the 1.2 mm thick one is inserted at a constant speed of 1 mm/s. The wedge is stopped after having traveled 20 mm, which corresponds to the beginning of the adhesive.

The jerky cracking caused by the continual sinking of the wedge makes it possible to study several phases of crack initiation and propagation, within the assembly. Optical profilometry measurements were carried out on the post-mortem facies 1, in order to quantify the surface roughness. The raw profiles presented in figures 2 allow a first comparison of the surface roughness: the mentions “Init”, P_1, P_2 and “Ouv” correspond respectively to the length of adhesive cracked during the initiation, to the lengths of adhesive cracked during the insertion of the wedge continuously, the test ends with the opening of the sample.

We apply a homological persistent analysis on the raw facies profiles at different scales in order to identify the level of roughness of the adhesives. The appearance of an extremely fractal profile at small scales for the most tenacious adhesive led us to investigate the height and the number of corresponding peaks.

3.2 Methodology

The following protocol is applied to the AHT and ABT M52 profiles: the raw profile is obtained by scanning a surface, which contains a number of lines. Once the surface is registered, the lines are averaged into a one-dimensional profile. This profile is then cut according to the events attributed to the crack jumps, which were determined by image correlation. The length of each crack jump, l, gives access to the minimum wave number, i.e. $k = 1/l$. The number of measurements is therefore very high, thus providing a lot of information, but even if the data can be viewed on a graph, a synthesis in a simple and unrepresentable descriptor is necessary.

With the corner continuously driven into the assembly, it causes jerky cracking in the adhesive. The principle of the measurement is based on the analysis of crack jumps caused by the insertion of the wedge continuously. For a mono-adhesive assembly, all the crack jumps are of the same length, they are visible and indicated in the figures by thin dotted lines. ABT adhesives have shorter seed lengths than AHT assemblies. According to the conclusions of Olivier Tramis's work [31], ABT M52 adhesives have a superior capacity to store the energy brought by the wedge during insertion. These adhesives also have lower crack jumps than AHT assemblies. This result is due in particular to a higher tenacity. ABT M52 assemblies therefore have superior adhesion. The rough profiles allow a first comparison of the surface roughness. The comparison is based on the maximum peak-to-peak amplitude of the small oscillations. The ABT assemblies tested have a raw surface condition that is, in principle, smoother than the AHT assemblies, which is in line with the observations of Chen et al. (Chen et al., 2001) [10]. ABT M52 adhesives have greater fracture resistance: more energy is needed to initiate a crack, and it is more difficult to propagate a crack. The crack propagating only in the joint, this increased resistance is attributed to a cohesion reinforced by the presence of copolymers. This also ties in with the fact that ABT adhesives are tougher..

The post mortem crack surfaces will be described by the heights of the profile peaks and the location of the crack jumps. In a first part, we want to compare and complete the experimental results through topological analysis. First we extract features using Vietoris-Rips filtration (see def 2.3) with all the persistence pairs 0-dimensional (H_0) (connected components) and 1-dimesional (H_1) (holes). We extract statistical features about the profiles (initiation, P_1, P_2) from lifetime diagrams. By taking a maximum height for the edges we include all the edges of length smaller than or equal to this value. The persistence diagrams give the evolution of the topological features of the crack. Peaks of roughness are persistent pairs in 0-th (H_0) dimensional lifetime diagrams 7 and 9 and the most persistent point correspond to a maximum height of the peak. The results are summarized in the table 2 and table 1. In a second time, we convert lifetime diagram

into persistence images for the H_1 points. In a third time, Bottleneck and Wasserstein distances was used to learn the similarity between two persistence diagrams. The interest in their use is based on the fact that these two distances are stable [12] : a small perturbation in the measured function creates a small perturbation in the persistence diagram. Then we are interested in the roughness both at the macro point of view and at the micro level, we computed the persistence diagrams at different scales. At the various scales, the number of connected components H_0 every $1\mu m$ is counted. At the micro scale, which corresponds to the number of peak, at the nano scale which will identify the number of voids, micro cracks. Indeed, zero dimensional features in the persistence diagram determine the persistency of the peaks in the raw profiles. Statistical information extracted from persistence diagrams on peak height will allow to compute the distribution of peaks at different scales and try to find power law behavior linking roughness with persistent diagram.

Furthermore, the roughness of the raw profiles of the ABT M52 and AHT adhesives seem to present periodicities. For the ABT M52 adhesive, the profile shows us fairly close periods, so we will speak of almost periodic, AHT adhesive exhibits two types of almost periodicity. For detecting the periodicity, we explore in a second part a method which uses sliding windows embedding (SWE) followed by homological persistence. The quantization is carried out by evaluating the circularity of a representation at the level of initiation, P_1 and P_2 jumps of the signal.

4 Results and discussion

4.1 Profile descriptors based on homology persistence

4.1.1 Lifetime diagram for the most persistent point

Peaks are points in the 0-th dimensional lifetime diagram and we look for the most persistent point. The maximum amplitude of the peak is given by the most persistent point for the initiation, P_1 and P_2 jumps see figure 7 and figure 9. Then we compare the amplitude of the peaks with the experimental results and the roughness conclusions. The topological signatures of TDA of the fracture profiles is computed with the Python library Ripser [30] and [3].

Table 2 and Table 1 confirm the experimental results of the maximum amplitudes: $300\mu m$ for AHT adhesive and $128\mu m$ for ABT M52 adhesive, (p 136 from O. Tramis's thesis). Peaks height for ABT adhesive seems to vary little, which implies that the profile is regular, there is very little difference between the initiation and propagation parts. Table 2 indicates that the maximum amplitude belong to the AHT adhesive, and amplitudes increase for each crack jump. Then the increase of the amplitude of the fluctuations

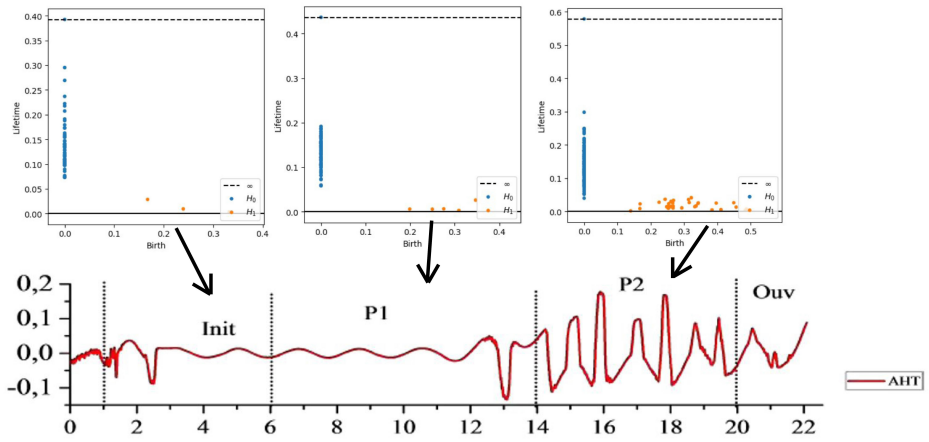

Figure 7: AHT adhesive lifetime diagrams for the different jumps of the raw profile. The blue dots in the diagrams above represent the birth and death values of points in the lifetime diagram in 0-dimensional and orange dots represent H_1 points.

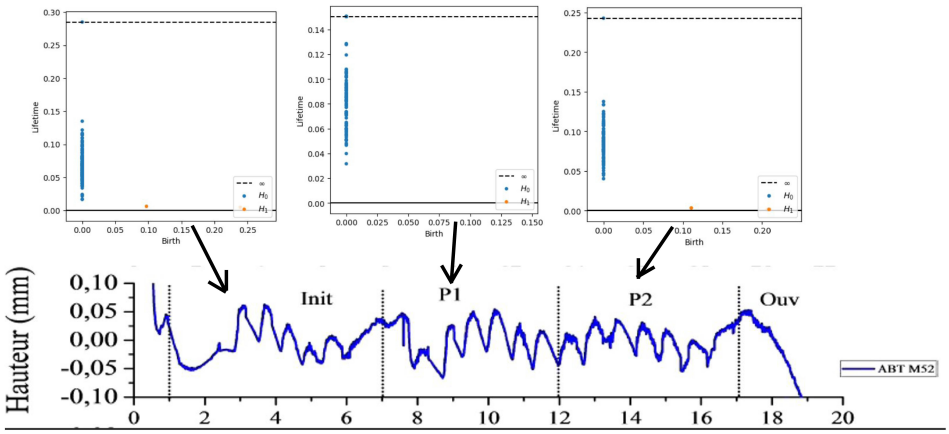

Figure 8: ABT M52 adhesive lifetime diagrams for the different jumps of the raw profile.

Table 1: Maximum amplitude of ABT adhesive.

ABT	Maximum peak amplitude
Initiation	128 μm
P_1	$128\mu m$
P_2	$127\mu m$

Table 2: Maximum amplitude of AHT adhesive.

AHT	Maximum peak amplitude
Initiation	$300\mu m$
P_1	$200\mu m$
P_2	$300\mu m$

induces an increase in the roughness in particular for the last jump.

4.1.2 Persistence images

Now we convert the birth lifetime diagram into persistence images. We place a Gaussian kernel on each point of component H_1 of the persistence diagram associated with a variable weighting function. We consider the micro-structures by choosing all the points of the persistence diagrams above the micron to create a pixelated version. We focus on the peaks of the profiles larger than $1\mu m$ and the features vectors are constructed by considering the maximum peaks. They are distinguished by pixel intensity. Persistent images are examined because they allow the persistence diagram to be vectorized. The vectors will be, in perspective, integrated into a neural network.

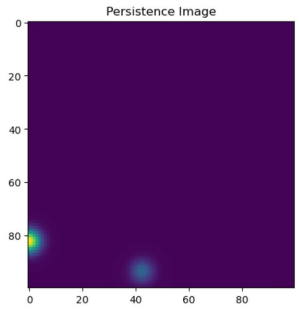

Figure 9: The H_1 persistent image of AHT initiation profile (resolution 100x100, $\sigma = 0.1$).

For the ABT adhesive, knowing that there are no persistent images for the jump P_1 in 1-dimensional, we obtain:

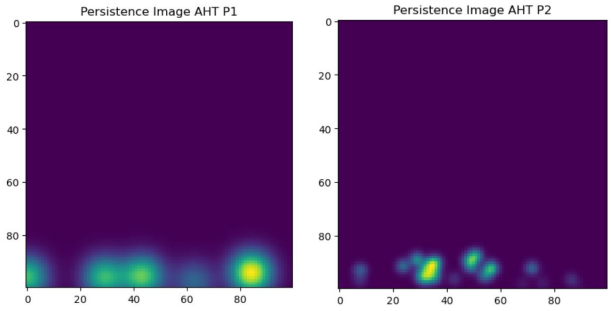

Figure 10: The H_1 persistent images of AHT for P1 and P2 profiles (resolution 100x100, $\sigma = 0.1$)

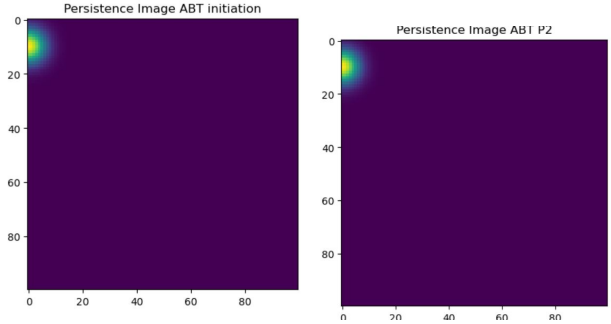

Figure 11: The H_1 persistent images of ABT initiation and P2 profiles (resolution 100x100, $\sigma = 0.1$)

4.1.3 Bottleneck and Wasserstein distances

Given the persistence diagram for each crack jump of the profiles, we use the Bottleneck and the Wasserstein distances between the two persistence diagrams (initiation - P_1 and P_1 - P_2) in order to compare the two persistence diagrams. These distances measure the similarity between the two persistence diagrams

We compute the Bottleneck and Wasserstein distances between their persistence diagrams for H_0 and H_1 points. For two persistence diagrams D_f and D_g, to measure their similarity, we consider bijections $\mu : D_f \to D_g$ The bottleneck distance between D_f and D_g is defined as,

$$d_B(D_f, D_g) = \inf_{\mu} \sup_{p \in D_f} \|p - \mu(p)\|_\infty \tag{14}$$

where the infimum is over all bijections from D_f and D_g.

The Wasserstein distance is defined as,

$$d_W(D_f, D_g) = \inf_{\mu} \sum_{p \in D_f} \|p - \mu(p)\|_\infty^k]^{\frac{1}{k}} \tag{15}$$

for any positive real number k.

Fig 12 shows the example of the persistence diagram for crack jump P_1 of ABT adhesive as well as the Bottleneck and Wasserstein distances between the two persistence diagrams of crack jump initiation and P_1.

The results of the two distances between the persistence diagrams for H_0 and H_1 points corresponding to the crack jump profiles of the two adhesives are summarized in the following tables:

Table 3: Bottleneck and Wasserstein distances for the H_0 points.

Persistence diagrams	Bottleneck distance	Wasserstein distance
(AHT) initiation - P_1	0.009	0.020
(AHT) P_1 - P_2	0.007	0.012
(ABT) initiation - P_1	0.007	0.023
(ABT) P_1 - P_2	0.012	0.035

The bottleneck distance captures the extreme behavior of topology features while the Wasserstein distance captures the average behavior. For two persistence diagrams obtained on a similar dataset of crack jump we should expect both distances to be close to zero. However, for the H_1 points of the AHT adhesive the Wasserstein distance is not close to zero, the ratio between the two distances varies from double (for initiation - P1) to quadruple (for P1 - P2). Unlike the ABT adhesive whose values are negligible for the H_1 points. For the H_0 points the Wasserstein distance for the AHT adhesive is

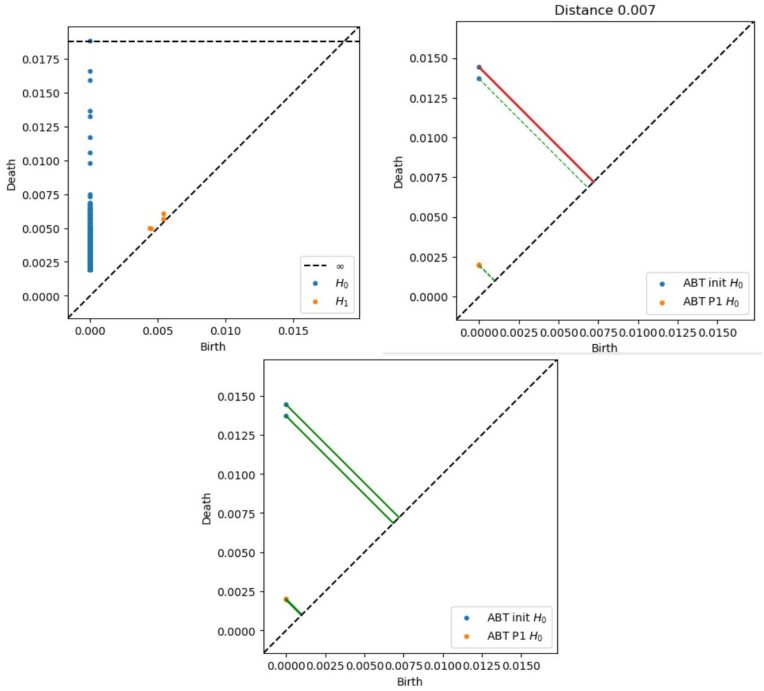

Figure 12: Persistence diagram of ABT M52 adhesive for the P_1 jump (left), Bottleneck distance representation between init and P_1 jump (right), and Wasserstein representation (bottom).

Table 4: Bottleneck and Wasserstein distances for the H_1 points.

Persistence diagrams	Bottleneck distance	Wasserstein distance
(AHT) initiation - P_1	0.084	0.16
(AHT) P_1 - P_2	0.033	0.14
(ABT) initiation - P_1	2.01e-04	1.6e-3
(ABT) P_1 - P_2	1.8e-04	9.5e-4

about twice the Bottleneck distances. While both distances are not negligible for ABT. Noting that the Wasserstein distance is 3 times the Bottleneck distance for ABT. The results of the Bottleneck and Wasserstein distances for the ABT adhesive for points H_0 and H_1 indicate similar persistence diagrams. While the results are somewhat less negligible for the AHT adhesive. In conclusion, the similarity of the ABT adhesive persistent diagrams implies that the crack jump profiles are close to each other. On the other hand, the difference noted for the AHT adhesive, particularly for the H_1 points, implies a less good similarity between the crack jumps, particularly in the

initiation and P_1.

4.1.4 Statistical information

Now, we want to count the number of peaks of the profiles, that is to say of connected components in 0-dimensional from the persistence diagrams, for this we use a sliding window on the profile of the adhesives of length $1mm$. We need to characterize the roughness of the profiles at different scales thanks to the distributions of the height fluctuations. We count of persistent pairs thanks to persistence diagrams for each scale in the ranges: above $1\mu m$, and below $1\mu m$. All the results can be found in the following tables:

Table 5: The number of peaks at the micro and nano level for ABT M52 adhesive. The number increases for the nano-level corresponding the micro-cracks.

Crack length of ABT	1mm	2mm	3mm	4mm	5mm	6mm	7mm	8mm	9mm
$0.01\mu m - 0.1\mu m$	482	459	462	467	452	456	471	475	463
$0.1\mu m - 1\mu m$	339	234	249	229	181	216	287	276	249
$> 1\mu m$	14	4	6	12	1	43	43	10	11

ABT	10mm	11mm	12mm	13mm	14mm	15mm	16mm	17mm
$0.01\mu m - 0.1\mu m$	473	459	456	437	455	438	448	476
$0.1\mu m - 1\mu m$	251	229	219	172	213	149	221	294
$> 1\mu m$	26	17	11	4	22	6	6	23

Table 6: The number of peaks at the micro and nano level for AHT adhesive. The number of peaks at the nano-level is half as many as ABT adhesive.

Crack length of AHT	1mm	2mm	3mm	4mm	5mm	6mm	7mm	8mm	9mm	10mm
$0.01\mu m - 0.1\mu m$	242	247	217	210	192	167	238	158	241	45
$0.1\mu m - 1\mu m$	186	210	83	71	22	19	30	19	172	45
$> 1\mu m$	41	29	1	1	1	1	1	1	1	1

AHT	11mm	12mm	13mm	14mm	15mm	16mm	17mm	18mm	19mm
$0.01\mu m - 0.1\mu m$	106	235	232	253	245	248	239	243	240
$0.1\mu m - 1\mu m$	106	135	153	153	190	190	200	210	192
$> 1\mu m$	1	48	33	53	54	41	64	40	45

The persistent pairs that are close to the diagonal represent nano-structures. The high number of these short-life pairs are formed by the short waviness

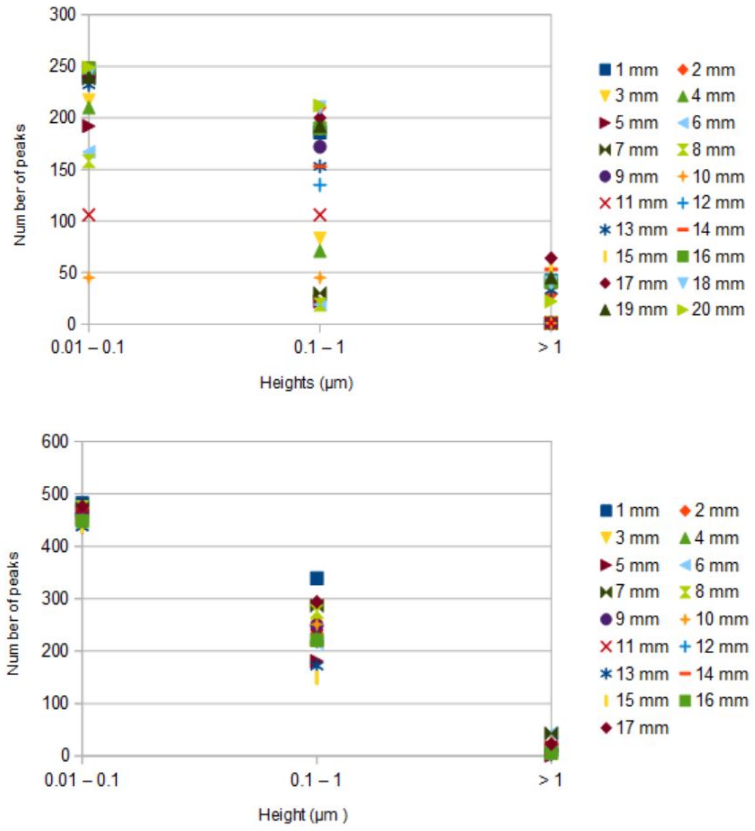

Figure 13: Distribution of the number of peaks at various scales for the AHT adhesive (top) and ABT adhesive (bottom). The abscissa corresponds to the different peak heights in micron, the ordinate represents the number of peaks.

at the surface. They tell us the presence of small-sized cavities and micro cracks, which results in small ripples at small scales. At first glance, we notice that the ABT adhesive, which is smoother than the AHT adhesive, has many fluctuations at the nano-scales. A smooth surface covered with heterogeneities can be more tenacious than a smooth surface allowing to reinforce an adhesive interface. Ghatak et al [16] showed that the peeling of an adhesive film is more difficult on a textured surface for which the textures are evenly distributed on the substrate. The increase in this toughness is explained by the fact that the dimension of the deformation zone at the crack tip is greater than the characteristic dimension of the textures which cover the surface. We want to show the correlation between the fluctuation in small scales and the tenacity of the adhesive.

For the AHT adhesive, Tables 6, between ranks $100\mu m - 1\mu m$, give us the general trend of the curve which is smooth and periodic for the initiation and the first crack jump. The number of connected components increasing from the second crack jump marking the increase in roughness. We also notice that the number of 0 dimensional pairs increase progressively for the nano-scales. Every millimeter (between 3 and 11 mm), the number of peaks above $1\mu m$ is equal to 1 which confirms the periodic nature visible on the AHT profile graph. Then the number of persistent pairs increases with decreasing scales. Moreover, they show that the number of nano-structures for ABT are more numerous than AHT adhesif. The high number of persistent pairs could be due to cavities, micro cracks. As ABT M52 adhesif is doped by copolymers, we can think that these nano particules reinforcing the tenacity of the ABT adhesive, are at the origin of these cavities, micro cracks. Moreover, it is noted that the number of nano-structures for the AHT adhesive are much less than for the ABT adhesive. This is explained by the fact that the AHT adhesive is not doped with copolymers. Hence, the AHT adhesive surface is soother in nano scale than the ABT M52 surface.

The distribution of the peak numbers at various scales for different crack lengths is shown on Figures 13 for the AHT, ABT adhesives for the post-mortem facies. The figure of the AHT adhesive shows us that in the micro level, the distribution is particularly scattered, which fits well with the chaotic profile of AHT. The distributions and the tables imply that the more the number of peaks decreases depending on the scale, the more their height and therefore their roughness increases. The distributions follow Yamamoto's constitutive law [32], which links the roughness and the persistence diagram of: $N(z) \propto z^{-\zeta}$ with $N(z)$ the number of peaks whose scale is larger or equal to z, and $\zeta = 2/\alpha$, α is then the roughness.

In conclusion of this first part, the homological persistence allowed to extract the main characteristics of the two mono-adhesives AHT and ABT M52. It was found that they were in agreement with the experimental results. Moreover, the multi-scale analysis of the persistence by counting the number of peaks at various scales made it possible to highlight the existence of cavities at the nano-level causing ripples on the structures. Faced with very large sets of data such as the raw profiles of adhesives, homological persistence makes it possible to simply synthesize their main characteristics which summarizes the multi-scale analysis carried out for each centimeter of crack. TDA sum up the topological structure of the high-dimensional data as it reduces the dimensionality of data.

4.2 Sliding windows and persistence homology

In this second part of the article, the interest focuses on the search for periodicity in the profiles. The goal is to identify the periodicity of the maximum peaks of the raw profiles in order to relate these results to Ghatak's

work [16, 17]. We want to clarify the link between cavitation, micro cracks in adhesives and the periodic nature of roughness peaks, by determining the average period. In [25] Perea et al. and [26] Perea and Harer introduce SWE used with persistent homology calculations in SW1PerS to quantify periodicity. Thanks to SWE and the persistence it allows them to classify the signals as periodic or not periodic and by periodicity alone. We use sliding windows embedding and persistence homology to show that AHT and ABT M52 adhesives are almost periodic and to define its period.

The depth of the crack is measured every $0.002mm$. Its fully ordered coordinates index and can be considered as a time series. The initiation, P_1 and P_2 raw profiles measured constitute finite time series composed by sequence of vectors $(x_0^{init}, x_1^{init}, ...)$, $((x_0^{P1}, x_1^{P1}, ...)$, $(x_0^{P2}, x_1^{P2}, ...)$. We use Takens' embedding theorem [28] to reconstruct a new time series, considering time delays and a sliding window embbeding which converts a time series into a cloud of points while keeping all the temporal information.

For the two parameters : the embedding dimension $d \geq 0$ and the time-delay τ where d is an integer greater than 1 and τ is a positive real number, we define the discretized sliding windows embedding starting at t as the vector:

$$SW_{d,\tau}x_t = [x_t, x_{t+\tau}, x_{t+2\tau}...x_{t+d\tau}] \in \mathbb{R}^{d+1} \tag{16}$$

for initiation, P_1 and P_2 jumps and where the sliding window size is defined by $d\tau$. We apply the work of Perea et al [26] which showed that maximum persistence, as a measure of the roundness of a point cloud, is obtained when the size of the sliding window corresponds to the length of the period of the signal. We choose this efficient method in order to identify the periodicity or quasi-periodicity of the ABT and AHT profiles as well as their period. The definition of the sliding window size is given by:

$$d\tau = (\frac{d}{d+1})\frac{2\pi}{L} \tag{17}$$

where L is the number of expected periods.

On the graphs, two distinct quasi-periods can be distinguished for the AHT adhesive and a single "rough" quasi-period of approximately $1mm$ for the ABT adhesive. Periodicity of the point cloud reveals the repetition of the patterns of the profiles. For a almost-periodic behavior the point cloud representation exhibits different topology. Then the next step is to calculate, on a finite sample, the n-dimensional persistence diagrams $n = 0, 1, 2$ via the Rips filtration. We used the code of a high performance topological machine learning toolbox in Python Giotto TDA [29] for the crack embedding, the n-dimensional persistence diagrams. In a 1-dimensional persistence diagram, circularity manifests as a point far from the diagonal.

We construct a SWE by setting the dimension to $d = 3$. It is then observed whether there is roundness of the cloud of points. Then we calculate

for d and τ the persistence diagrams (PD) of the cloud of points of the SWE, of dimensions 0, 1 and 2. L is determined by counting the number of H_1 points (holes)in the persistence diagrams furthest from the diagonal, with the closest points being considered noise and not counted. We can calculate for the sample of initiation, P_1 and P_2 jumps of the two adhesives, the size of the sliding window given by the definition above of Perea et al. If the profile is periodic the roundness of $SW_{d,\tau}x_t$ maximized when the window-size approaches the period length.

We present Fig 14 and 15 the representation of the application of Takens theorem on the point clouds of ABT, AHT adhesives and their corresponding persistence diagrams. For example, the sample for the P_2 jump of ABT M52 contains 2546 points, a period is identified by approximately 328 points. We evaluate the $SW_{d\tau}X(t)$ by fixing $d = 3$ and choosing time delay depending on the representation and roundness of the point cloud. Then we downsample the original data point clouds by selecting 846 points to more easily extract topological features. The process continues with the computation of Rips persistence diagrams of $SW_{d\tau}X(t)$ in dimension $n = 0, 1, 2$ with particular interest in the result in 1 dimension.

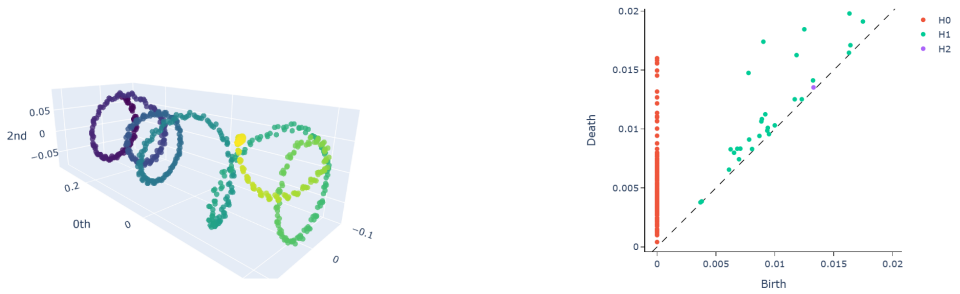

Figure 14: Top left: Representation of point cloud of ABT for the P_2 jump and on the right the associated persistence diagram is shown.

Nearly periodic peaks at large amplitudes produce a larger scale 1 cycle corresponding to the furthest points in the persistence diagram, small oscillations at the smallest scales are found closest to the diagonal of the diagram. We note that the data of the ABT adhesive reveal five points H_1 and one point H_2, but two points associated with 1-dimensional persistent homology H_1 and one point associated with 2-dimensional persistent homology H_2 at the top of the persistence diagram is the signature of a torus. Associated with these persistent points in the diagrams are the cluster points closest to the birth-death diagonal representing the white noise.

Finally, we determine the length of the period thanks to the SWE and their embedding parameters which are summarized in the tables.

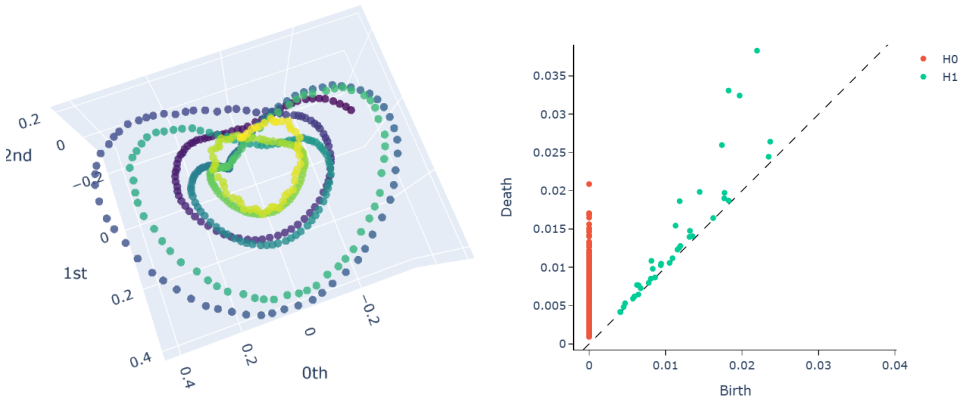

Figure 15: Point cloud from Takens embedding of AHT adhesive and its corresponding persistence diagram for the P_2 jump

Table 7: Sliding windows embedding size of ABT adhesive.

ABT	initiation	P1	P2
d	3	3	3
L	6	4	5
SWE size (mm)	1.04	1.17	0.94

Table 8: Sliding windows embedding size of ABT M52 adhesive.

AHT	initiation	P1	P2
d	3	3	3
L	2	2	7
SWE size (mm)	2.4	2.04	0.7

Based on the study of the detachment of a flexible plate from a thin textured adhesive film. Ghatak et al. [17] find that the initiation and propagation of cracks, from incision, in these thin adhesive films would be due to the nucleation of cavitation bubbles behind the contact line which increase the load necessary for peeling by creating a crack front. Then the bubbles grow and merge until a viable crack propagates. They show that a textured elastic film pattern on a length scale less than or equal to the stress decay length leads to a significant increase in interfacial toughness. It is noted that the peeling or separation moment as a function of displacement shows a linear increase in load followed by softening associated with the formation, and growth of cavitations over a period of approximately 1 mm. In a previous study, Ghatak and Chaudhury [16] showed that cavitations did not

occur randomly but were rather the consequence of instabilities leading to the formation of periodically spaced bubbles with a wavelength of 4 times the film thickness.

These results should be compared with those of the ABT M52 adhesive which effectively has the highest cavitation contribution as well as an increased resistance to cracking. In addition, the period length of a roughness peak according to the Table 7 is on average equivalent to $1mm$.It has been seen in the experimental study that the addition of particles makes it possible to reinforce the tenacity of the adhesives. One of the possible reinforcement mechanisms lies in the creation of micro-voids (it is possible to see micro-cracks as voids), cavities. In this case, the adhesive that best resists cavitation in the gel state should resist the best crack propagation in the structural state.

5 Conclusion and perspectives

The structural properties of ABT M52 and AHT adhesives were evaluated using a cleavage test. The topological characteristics of the rupture facies are identified thanks to the persistence diagrams in order to evaluate the fluctuations of the raw profile. The persistence diagrams made it possible to quantify the roughness at various scales: at the nano level were able to show the existence of voids, cavities, micro-fissures which are the consequences of the addition of micro particles such as copolymers. As well as at the micro level, we were able to highlight the smooth or rough passages of the surfaces.

The number of zero-dimensional pairs in the persistence diagrams at the micro-scale provide evidence of roughness : they count the number of peaks of the micro level waviness of the profiles. The number of peaks is very high at the nano level then a significant drop at the micro level translated by Yamamoto's power law behaviour, which reveals the increase in roughness. Moreover, the zero-dimensional pairs at the micro-level in the persistence diagram, far from the diagonal, characterize the number of peaks at maximum amplitudes of the profiles and confirm the experimental results of the maximum amplitudes. The pairs at the nano level characterize the voids, the micro-cracks which lead to waviness of the profiles. The topological analysis of data made it possible to synthesize and summarize all the main and multi-scale characteristics resulting from the raw profiles.

We also consider another approach which consists of vectorizing the persistence diagram by converting it into a persistence image. It is particularly suited to machine learning problems. The study of similarity of persistent diagrams using Bottleneck and Wasserstein distances and the sliding window embedding method confirm through homology the quasi-periodic and regular profile of the ABT M52 adhesive compared to the much rougher and irregular profile of AHT. Experimentally it is shown that ABT M52 is more

resistant to fracture and higher toughness than AHT. However, the presence of cavitations, of micro cracks quantified using TDA, in ABT M52 creates resistance to cracking.

In perspective, the vectorization of persistence diagrams in the first part of the article allows them to be converted into more practical structures. Machine Learning will be applied to the feature vectors of each persistence diagram. It will be interesting to inject these feature vectors into an artificial neural network in order to study and predict the characteristics of no longer mono-adhesive assemblies but of hybrid joints bringing together the two principles of ABT M52 and AHT configurations.

References

[1] H. Adams, S. Chepushtanova, et al., Persistence images: A stable vector representation of persistent homology, *J. Mach. Learn. Res.*, **18** (2017), Paper No. 8, 35 pp.

[2] K. B. Armstrong, Long-term durability in water of aluminium alloy adhesive joints bonded with epoxy adhesives, *International Journal of Adhesion and Adhesives*, **17** (1997), 89-105.

[3] U. Bauer, Ripser: Efficient computation of Vietoris-Rips persistence barcodes, *J. Appl. Comput. Topol.*, **5** (2021), 391-423.

[4] P. Bubenik, Statistical topological data analysis using persistence landscapes, *Journal of Machine Learning Research*, **16** (2015), 77-102.

[5] J. C. Bolger, et al., Adhesives in manufacturing, *Marcel Dekker, Inc.*, (1983).

[6] P. Bubenik and P. Dłotko, A persistence landscapes toolbox for topological statistics, *J. Symb. Comput.*, **78** (2017), 91-114.

[7] H. Canot, et al., Prediction the strain of traction-aged polymer systems from artificial neural networks with regularization, *IAENG International Journal of Computer Science*, **49** (2022), 4.

[8] https://geometrica.saclay.inria.fr/team/Fred.Chazal/.

[9] F. Chazal, B. T. Fasy, F. Lecci, B. Michel, A. Rinaldo and L. Wasserman, Subsampling methods for persistent homology, *ICML 15: Proceedings of the 32nd International Conference on International Conference on Machine Learning*, **37** (2015), 2143-2151.

[10] B. Chen, et al., Crack path selection in adhesively bonded joints: The role of material properties, *The Journal of Adhesion*, **75** (2001), 405-434.

[11] J. Cognard, Influence of water on the cleavage of adhesive joints, *International Journal of Adhesion and Adhesives*, **8** (1988), 93-99.

[12] D. Cohen-Steiner, H. Edelsbrunner and J. Harer, Stability of persistence diagrams, *Discrete Computational Geometry*, **37** (2007), 103-120.

[13] D. A. Dillard, et al., On the use of a driven wedge test to acquire dynamic fracture energies of bonded beam specimens, *The Journal of Adhesion*, **87** (2011), 395-423.

[14] A. N. Duman, B. S. Yilbas, H. Pirim and H. Ali, Texture analysis of hydrophobic polycarbonate and polydimethylsiloxane surfaces via persistent homology, *Coatings*, **7** (2017), 139.

[15] R. Forman, Morse theory for cell complexes, *Advances in Mathematics*, **134** (1998), 90-145.

[16] A. Ghatak and M. K. Chaudhury, Adhesion induced instability patterns in thin confined elastic film, *Langmuir*, **19** (2003), 2621-2631.

[17] A. Ghatak, L. Mahadevan, Y. Chung Jun, K. Chaudhury Manoj and V. Shenoy, Peeling from a biomimetically patterned thin elastic film, *Proc. R. Soc. Lond. A.*, **460** (2004), 2725-2735.

[18] S. R. Hartshor, Structural Adhesives: Chemistry and Technology, Sous la dir. de S R Hartshorn, 3rd, New York, Plenum Press, 1986.

[19] M. S. Hasan and M. Nosonovsky, Triboinformatics: Machine learning algorithms and data topology methods for tribology, *Surface Innovations*, **10** (2022), 229-242.

[20] L. J. Hart-Smith, The strength of adhesive bonded single lap joints, *Douglas Aircraft Company IRAD Technical Report MDC*, (1970), J0472.

[21] L. J. Hart-Smith, A peel-type durability test coupon to assess interfaces in bonded, co-bonded, and co-cured composite structures, *International Journal of Adhesion and Adhesives*, **19** (1999), 181-191.

[22] C. Maria, J.-D. Boissonnat, M. Glisse and M. Yvinec, The gudhi library: Simplicial complexes and persistent homology, *International Congress on Mathematical Software (Springer)*, (2014), 167-174.

[23] R. A. Pearson, et al., Influence of particle size and particle size distribution on toughening mechanisms in rubber-modified epoxies, *J. Mater. Sci.*, **26** (1991), 3828-3844.

[24] R. A. Pearson, et al., Toughening mechanisms in thermoplasticmodified epoxies: 1. Modification using poly (phenylene oxide), *Polymer*, **34** (1993), 3658-3670.

[25] J. A. Perea, A. Deckard, S. B. Haase and J. Harer, SW1PerS: Sliding windows and 1-persistence scoring; discovering periodicity in gene expression time series data, *BMC Bioinformatics*, **16** (2015), 257.

[26] J. A. Perea and J. Harer, Sliding windows and persistence: An application of topological methods to signal analysis, *Foundations of Computational Mathematics*, **15** (2015), 799-838.

[27] J. F. Senge, A. H. Astaraee, P. Dłotko, et al., Extending conventional surface roughness ISO parameters using topological data analysis for shot peened surfaces, *Sci. Rep.*, **12** (2022), 5538.

[28] F. Takens, Detecting strange attractors in turbulence, in D. A. Rand and L. S. Young, *Dynamical Systems and Turbulence*, Warwick, 1980. *Lecture Notes in Mathematics*, Springer- Verlag, **898**, 366-381.

[29] G. Tauzin, et al., Giotto-tda: A topological data analysis toolkit for machine learning and data exploration, *J. Mach. Learn. Res.*, **22** (2021), Paper No. 39, 6 pp.

[30] C. Tralie, N. Saul and R. Bar-On, Ripser.py: A Lean persistent homology library for python, *Journal Of Open Source Software*, **3** (2018), 925.

[31] O. Tramis, *Méthodologies de Caractérisation de L'adhérence D'assemblages Collés. Application à la Caractèrisation d'un Joint adhésif à Gradient de Propriétés*, Thesis, INP Toulouse, 2016.

[32] K. Yamamoto, Topological analysis of rough surfaces using persistent homology, *J. Phys. Soc. Jpn.*, **84** (2015), 113001.

[33] A. F. Yee, et al., Toughening mechanisms in elastomer-modified epoxies - Part 1 Mechanical studies, *Journal of Materials Science*, **21** (1986), 2462-2474.

[34] M. Yesilli and F. Khasawneh, Data-driven and automatic surface texture analysis using persistent homology, *2021 20th IEEE International Conference on Machine Learning and Applications (ICMLA)*, Pasadena, CA, USA, (2021), 1350-1356.